ARTICLE

Bioactive Glass 45S5 Powders: Effect of Synthesis Route and Resultant Surface Chemistry and Crystallinity on Protein Adsorption from Human Plasma

Markian S. Bahniuk · Hamidreza Pirayesh · Harsh D. Singh · John A. Nychka · Larry D. Unsworth

Abstract Despite its medical applications, the mechanisms responsible for the osseointegration of bioactive glass (45S5) have yet to be fully understood. Evidence suggests that the strongest predictor for osseointegration of bioactive glasses, and ceramics, with bone tissue as the formation of an apatitic calcium phosphate layer atop the implanted material, with osteoblasts being the main mediator for new bone formation. Most have tried to understand the formation of this apatitic calcium phosphate layer, and other bioresponses between the host and bioactive glass 45S5 using Simulated Body Fluid; a solution containing ion concentrations similar to that found in human plasma without the presence of proteins. However, it is likely that cell attachment is probably largely mediated via the adsorbed protein layer. Plasma protein adsorption at the tissue bioactive glass interface has been largely overlooked. Herein, we compare crystalline and amorphous bioactive glass 45S5, in both melt-derived as well as sol–gel forms. Thus, allowing for a detailed understanding of both the role of crystallinity and powder morphology on surface ions, and plasma protein adsorption. It was found that sol–gel 45S5 powders, regardless of crystallinity, adsorbed 3–5 times as much protein as the crystalline melt-derived counterpart, as well as a greater variety of plasma proteins. The devitrification of melt-cast 45S5 resulted in only small differences in the amount and variety of the adsorbed proteome. Surface properties, and not material crystallinity, play a role in directing protein adsorption phenomena for bioactive glasses given the differences found between crystalline melt-cast 45S5 and sol–gel derived 45S5.

1 Introduction

Bioactive glasses, specifically ceramic Bioglass® formulation 45S5 (45 %SiO_2, 24.5 %Na_2O, 24.5 %CaO, and 6 % P_2O_5 by weight), have garnered serious attention as a functional biomaterial due to its ability to integrate with bone. Previous work has shown that bioactive glass 45S5 can be inserted into areas of large scale bone damage to help augment its repair, while providing structural support by binding strongly to endogenous bone [1–3]. This material is capable of interacting with the surrounding tissue milieu, and has been shown to serve as a substrate on which osteogenic stem cells can attach and differentiate [2–8]. Moreover, bioactive glasses have been used for several clinical applications, such as ossicular implantation for alleviating conductive hearing loss, as dental implants for maintaining the endosseous ridge before dentures are fitted, and as a particulate for augmenting the natural repair process in patients with periodontal disease [9]. Besides improving the mechanical properties of the final material, leading to its application to a broader range of clinical applications, inducing crystallinity in bioactive glasses may

M. S. Bahniuk · L. D. Unsworth
Department of Biomedical Engineering, Faculty of Medicine, University of Alberta, Edmonton, AB T6G 2V4, Canada

M. S. Bahniuk · L. D. Unsworth
National Institute for Nanotechnology, National Research Council (Canada), Edmonton, AB T6G 2M9, Canada

H. Pirayesh · H. D. Singh · J. A. Nychka (✉) ·
L. D. Unsworth (✉)
Department of Chemical and Materials Engineering, Faculty of Engineering, University of Alberta, Edmonton, AB T6G 2V4, Canada
e-mail: jnychka@ualberta.ca

L. D. Unsworth
e-mail: lunswort@ualberta.ca

affect the mineral formation rate and bone integration at the tissue-material interface [10–12]. Nonetheless, clear evidence implicates the strongest predictor for osseointegration of bioactive glasses and ceramics with bone tissue as the formation of an apatitic calcium phosphate layer atop the implanted material, as aptly reviewed elsewhere [13]. Wherein, strong in vivo evidence suggests that osteoblasts, in the presence of an apatitic calcium phosphate layer, attach and proliferate to form new bone. Most work in the field has tried to model the interaction between the host and bioactive glass 45S5 using Simulated Body Fluid (SBF) rather than in vivo testing. Kokubo and Takadama posit that a particular concentration of ions in a simulated body fluid (SBF, with ion concentrations similar to those found in human plasma) may be useful in predicting in vivo bone formation if an apatitic calcium phosphate layer forms on the surface of the bioactive glass after immersion in the SBF [13]. The situation is of course more complicated: cells may not directly attach to these surfaces, rather cell attachment may largely be mediated via adsorbed proteins, and SBF contains no proteins. It appears that the adsorption of proteins at the tissue bioactive glass interface has been largely overlooked regarding proxy tests for in vivo animal implantation and histology.

The crystallinity and the manufacturing method of 45S5 are thought to have significant effects on this material [11, 12]. Many studies have investigated the effect of devitrifying bioactive glasses, to move from an amorphous to ceramic glass (crystalline or semi-crystalline), so as to optimize the required parameters of bioactive materials for application in the medical industry: with a special emphasis on bone growth [14–16]. Bioactive glass 45S5 transforms to a glass ceramic with crystalline phase $Na_2Ca_2Si_3O_9$ (combeite) by heating the material at 700 °C for more than 0.5 h [17, 18]. Crystallization of the bioactive glass results in improved mechanical properties and allows for powder sintering. Despite these benefits, glass ceramics (crystalline or semi-crystalline) can show less solubility in body fluid and, thus, may dramatically affect the protein adsorption profile. Various mechanisms for such in vitro and in vivo behavioural differences have been proposed. A common argument is that the phosphorous concentration and distribution changes upon crystallization of a glass, and thus the phosphorous dissolution profile changes, which ultimately affects the time to form a mineral phase suitable for tissue integration (i.e., hydroxycarbonate apatite, HCA). For example, crystalline ceramics of the same starting composition require three times as much time to form HCA compared to amorphous counterparts [12]. Such a time limitation to form HCA for crystalline ceramics can be overcome by increasing the surface area of the material by using an alternate manufacturing method [19] in order to change the "texture" of the ceramic [20]. As opposed to the dense surface structure created via traditional melt casting methods, the sol–gel method is a widely used production technique that yields a highly porous material structure, which could lead to higher apparent dissolution rates (higher surface area to volume ratio) [21].

The interactions of bioactive glass ceramics with the host environment have been characterized using either SBF or cell studies. SBF is an acellular solution designed to mimic the ionic concentrations of various elements found in human plasma including Na^+, Mg^{2+}, Ca^{2+}, Cl^-, HCO_3^- and HPO_4^{2-} [22]. However, it lacks other plasma components such as dissolved nutrients, vitamins, triglycerides, cholesterols and proteins. This omission may be why cell studies with bioactive glasses show results ranging from enhancement of bone repair to inhibition of the same process [23–27]. While proteins make up less than 10 % of human plasma, their effects on host response can outweigh any effect elicited by a change in ion concentration. The adsorption of a protein layer to a biomaterial surface takes mere seconds, but this adsorbed layer directs any host responses such as platelet activation, coagulation, complement and immune responses as well as any interactions between cells and the biomaterial [28].

It has been shown in the literature that the presence of proteins can affect 45S5 bioactive glass reactions yet the interactions of plasma proteins with 45S5 bioactive glass have not been studied in depth. Most studies make use of either single or double protein solutions or do not attempt to identify which proteins adsorb to the bioactive glass surface [23, 29, 30]. Understanding the complex adsorption phenomena and their effects on host response is critical to our understanding of all bioactive glasses, including 45S5. To this end, this study will examine the adsorption of proteins from platelet-poor human plasma to most accurately simulate the adsorption effects seen when the bioactive glass is used in medical applications. Furthermore, immunoblots will be used to reliably identify the types of proteins found eluted off of the surfaces down to picomolar concentrations. The consequences of changes in bioactive glass formulations as well as any underlying crystalline domains may alter plasma protein adsorption and also need to be understood. This knowledge is important not only for the development of bioactive glasses, but because of 45S5's clinical successes, the plasma adsorption information can be used in the development of a generalized model of plasma protein adsorption to all biomaterial surfaces.

In this study a comparison of the protein absorption from human blood plasma to melt-cast 45S5 (amorphous and crystalline), with gel-derived 45S5 (crystalline), has been carried out. It was found that the gel-derived glass had about twice the specific surface area (using BET-N_2

adsorption techniques) of the cast samples due to the submicron porosity demonstrated by SEM. XPS analysis showed there was a difference in surface compositions between the amorphous and crystalline samples but the surface charges for each sample were all around -15 mV. The sol–gel bioactive glass eluted 3–5 times more protein than the cast samples and also showed a greater variety of plasma proteins in the adsorbed proteome. It appears that the atomic surface composition of the materials has a greater effect on protein adsorption than net charge, as well as material crystallinity.

2 Materials and Methods

2.1 Materials

Bioactive glass 45S5 prepared by two separate manufacturing routes (melt and sol–gel derived) was used in this study. Melt-derived bioactive glass 45S5 powder (<20 μm) was furnished by Mo-Sci Corporation (Missouri, USA). Two versions of melt-derived 45S5 were used: amorphous (as received) and crystalline (devitrified). Crystalline 45S5 was prepared by heat treating amorphous glass powder at 720 °C for 20 min which resulted in 100 % crystalline 45S5.

Sol–gel derived glasses were prepared according to the following procedure to prepare 20 g of powder. 3.26 mL of 69 % nitric acid was added to 47.6 mL of water to create a 1 M nitric acid solution. 0.15 mol (33.5 mL) tetraethylorthosilicate (TEOS, Sigma Aldrich, US) was added to the 1 M nitric acid for a final H_2O: TEOS molar ratio equal to 18. The precursor hydrolysis was performed for 60 min with stirring. The following reagents were allowed to react for 45 min during stirring in the following sequence: 0.017 mol (2.9 mL) triethylphosphate (TEP, Sigma Aldrich, US), 0.085 mol (20.13 g) calcium nitrate tetrahydrate (Sigma Aldrich, US), and 0.16 mol (13.52 g) sodium nitrate (Sigma Aldrich, US). The prepared transparent solution was stored in a sealed Teflon container for 5 days at ambient temperature to allow gel formation. The gel was aged for 24 h at 70 °C then dried at 120 °C for 24 h. Finally the dried sample was stabilized in a high alumina crucible at 700 °C using a benchtop muffle furnace (Thermo scientific, F48055-60) for 24 h to remove residual nitrates. The prepared powder was ground using a planetary ball-mill at 500 rpm for 10 min with a spherical zirconia media (2 mm dia.) in ethanol to reduce the particle size to 5–15 μm in order to be comparable to that of the melt-cast powders. Measurement of particle size was carried out by photon correlation spectroscopy [31]. The average median diameter of melt cast and gel-derived powders were 8.0 and 11.8 μm, respectively.

2.2 Surface Area Measurement

The surface areas of the powders were measured using a Quantochrome Autosorb MP1 (Florida, USA) automatic gas absorption system. The measurements were carried out using nitrogen isotherms at 77 K. The point BET method (0.05, 0.075, 0.1, 0.15, 0.25 and 0.3 mm Hg) was used to analyze data. All the samples were degassed at 200 °C, under vacuum, for 3–4 h prior to the tests. All values returned using the BET method have an associated error of 5 %.

2.3 Scanning Electron Microscopy

A JEOL 6301F scanning electron microscope (SEM, Tokyo, Japan) was used to image the morphology of the powder particles. Samples were coated with chromium to achieve the highest conductivity with the least charging (Edwards XE200, Xenosput, Australia). A 5 kV accelerating voltage was also used to minimize charging.

2.4 X-ray Diffraction

A Rigaku Rotaflex Diffractometer (Woodlands, TX, USA) was used to carry out X-ray diffraction (XRD) to characterize the powder morphology and identify the presence of crystalline phases after devitrification of bioactive glass. The diffractometer was operated at 40 kV and 110 mA (Cu target) at 2θ range of 10–110° with a step size of 0.02°.

2.5 Zeta-Potential Analysis

The electrophoretic mobility of the bioactive glass samples was measured using the Nano-ZS instrument (Malvern Instruments Ltd., UK) at 25 °C in order to determine their surface charges. If necessary, samples were diluted with 1 mM NaCl solution.

2.6 X-ray Photoelectron (XPS) Analysis

The XPS measurements were performed using an AXIS 165 spectrometer (Kratos Analytical) at the Alberta Centre for Surface Engineering and Science (University of Alberta). The base pressure in the analytical chamber was lower than 3×10^{-8} Pa. A monochromatic Al K α source ($hv = 1486.6$ eV) was used at a power of 210 W. The analysis spot was 400×700 μm. The instrument resolution was 0.55 eV for Ag 3d and 0.70 eV for Au 4f peaks. Survey scans were collected for binding energy from 1100 eV to 0 with analyzer pass energy of 160 eV and a step of 0.35 eV. High-resolution spectra pass-energy was 20 eV with steps of 0.1 eV. The number of scans varied from 8 to 60. Electron flooding was applied to compensate

for sample charging. The binding energies of all samples were corrected using 284.8 eV for the C1 s peak.

High-resolution Si spectra were modeled using Casa-XPS (version 2.3.15, Casa Software Ltd.). The Si model contained two components: one component representing SiO, where the peak position, but not full-width at half maximum (fwhm), was fixed at a value of 102.7 eV [32]. A second component was represented via the addition of another peak; this peak was left unconstrained and was identified using data from the National Institute of Standards and Technology (NIST) X-ray Photoelectron Spectroscopy Database (http://srdata.nist.gov/xps/Default.aspx).

2.7 Plasma Adsorption

Platelet poor human plasma was obtained from the Research Division of Canadian Blood Services and stored at −80 °C prior to its use. Bioactive glass materials were added to 0.15 M phosphate buffered saline (PBS). In order to compare protein adsorption results between the various bioactive glass samples, surface area values for each system were characterized using BET analysis (as outlined above). That said, it should be recognized that (esp. for sol–gel samples) BET results for surface area is directly relative to the size of nitrogen and may significantly overestimate how much surface area is accessible to protein for adsorption. 250 μL of each bioactive glass solution were mixed with 1.25 mL human plasma for a final plasma concentration of 83 %. Protein adsorption was conducted at 37 °C for 2 h under rocking agitation. Samples were spun down at 13,000 rpm (VWR galaxy 16DH, Mississauga, ON) for 10 min. Supernatant was replaced with 1 mL 0.15 M PBS, left at room temperature for 30 min so as to remove loosely bound proteins. This wash step was carried out twice.

Adsorbed protein was eluted from the bioactive glass surface by incubating rinsed samples in 2 % w/v sodium dodecyl sulfate (SDS) (J.T. Baker, Phillipsburg NJ) in 0.15 M PBS at 50 °C for 2 h as described in [33]. Conditions that yielded consistent and optimal protein removal included looking at temperature variation (room temperature to 50 °C) and solution SDS concentration (2–10 %). The above strategy was found to be optimal (results not shown). Eluent containing removed protein was collected by centrifuging the samples, as described above. Finally, all blood donors were fully informed (according to Canadian Blood Services policy) and samples were pooled to anonymize the donors.

2.8 Total Protein Assays

The DC Protein Assay from Bio-Rad (Hercules, CA) was used to determine the concentration of eluted protein from the bioactive glass samples. Recommended manufacturer's

protocols were followed. Briefly, bovine serum albumin (BSA) was used to generate standard curves in 2 % SDS and 0.15 M PBS. The BSA control and 100 μL aliquots of each solution of protein eluted from the bioactive glass sample were analyzed using the protein assay kit components, and a DU 730 Life Sciences UV/Vis spectrophotometer (Beckman Coulter, Mississauga, ON) was used to read the absorbances at 740 nm. Each sample was assayed in duplicate.

However, for some samples the total protein values returned from this assay were near the assay's lower limit, questioning their accuracy. Thus, an alternative method was developed based on colloidal gold staining [23], which should have a significantly greater sensitivity to the protein. 3 μL from each bioactive glass sample was pipetted onto a PVDF membrane (0.2 μm, Bio-Rad, Hercules, CA) and allowed to air dry. The same was done with various known quantities of BSA in the same buffer as the samples. The membranes were then processed according to the Colloidal Gold Total Protein Stain instructions (Bio-Rad, Hercules CA). Briefly, the membranes were blocked with 0.3 % Tween 20 in Tris-buffered saline (20 mM Tris and 500 mM NaCl) three times for 20 min each, rinsed with Milli-Q Synthesis purified water (Billerica, MA) 3 times for 2 min each, stained with colloidal gold solution (Bio-Rad, Hercules, CA) for 1 h and finally rinsed again with purified water 3 times for 1 min each. The membranes were then scanned and the stain intensities, less background intensities, quantified using Adobe Photoshop (Version 9, Adobe Systems Inc, San Jose CA USA). This information, coupled with the calibration curve intensities, yielded the total protein per sample.

2.9 SDS-PAGE and Western Blotting

As described previously [34], 30 μg of total eluted protein from each bioactive glass sample was analyzed using reducing SDS polyacrylamide gel electrophoresis (SDS-PAGE) and Western blotting techniques. Briefly, protein samples were reduced and denatured by the addition of sample buffer which, when diluted, contained 0.5 M β-mercaptoethanol and 2 % SDS. The sample and sample buffer mixtures were then heated at 95 °C for 5 min before being run on 12 % SDS polyacrylamide gels at 200 V and 400 mA. Proteins were transferred from these gels to 0.2 μm Immuno-Blot PVDF membrane (Bio-Rad, Hercules, CA) for 1 h at 100 V, 200 mA. All consumables and equipment were purchased from Bio-Rad (Hercules, CA). The membranes were then divided into strips for colloidal gold staining or Western blotting. Table 1 lists the primary and secondary antibodies used for Western analysis. The antibodies were used without further purification at concentrations of 1:1000. 350 μL of stabilized TMB substrate

Table 1 Primary antibodies used for immunoblotting of plasma proteins adsorbed to bioactive glass as well as plasma protein physical characteristics

Antibody	Plasma protein MW (kDa)	Plasma protein pI	Host	Source
Kininogen (light chain)	50	6.6	Mouse	US Biological, Swampscott, MA, USA
Kininogen (heavy chain)	88–120	6.8	Mouse	US Biological, Swampscott, MA, USA
Factor I	88	7.6	Mouse	Cedarlane Laboratories, Hornby, ON, CAN
Fibrinogen	340	6.6	Rabbit	Calbiochem, Gibbstown, NJ, USA
Fibronectin	440	5.7	Rabbit	Cedarlane Laboratories, Hornby, ON, CAN
Hemoglobin	68	8.0	Rabbit	Sigma-Aldrich, St. Louis, MO, USA
α_1-Antitrypsin	47	5.6	Sheep	Cedarlane Laboratories, Hornby, ON, CAN
Thrombin	36	5.4	Sheep	Cedarlane Laboratories, ON, CAN
Prothrombin	72	5.9	Sheep	Cedarlane Laboratories, ON, CAN
Protein C	62	6.3	Sheep	Cedarlane Laboratories, ON, CAN
Vitronectin	75	5.8	Sheep	Cedarlane Laboratories, ON, CAN
Protein S	69	5.7	Sheep	Cedarlane Laboratories, ON, CAN
Prekallikrein	85	8.2	Sheep	Cedarlane Laboratories, ON, CAN
Antithrombin	53	6.7	Sheep	Cedarlane Laboratories, ON, CAN
IgG	174	8.4	Goat	Sigma-Aldrich, St. Louis, MO, USA
Human albumin	66	6.8	Goat	OEM Concepts, Saco, ME, USA
Plasminogen	90	7.3	Goat	Cedarlane Laboratories, ON, CAN
Complement factor 3 (C3)	185	6.4	Goat	Calbiochem, Gibbstown, NJ, USA
Factor XII	80	7.7	Goat	Cedarlane Laboratories, ON, CAN
Factor XI	160	8.1	Goat	Cedarlane Laboratories, ON, CAN
Apolipoprotein A1	28	7.1	Goat	Sigma-Aldrich, St. Louis, MO, USA
Transferrin	77	7.1	Goat	Sigma-Aldrich, St. Louis, MO, USA
α_2-Macroglobulin	718	6.4	Goat	Sigma-Aldrich, St. Louis, MO, USA

(Promega, Madison, WI) was used to visualize all protein-antibody complexes. The colour developing reactions were allowed to progress until precipitation of the coloured compound was observed (20 min for cast amorphous and cast crystalline and 10 min for sol–gel). The reaction was then quenched for 10 min with 2 mL of water from a MilliQ Synthesis water purification system (Billerica, MA).

3 Results

3.1 Surface Area

Surface area measurements were performed on both the melt-cast and sol–gel derived bioactive glasses in order to determine if the surface areas per gram changed as a function of the manufacturing method. It was found that the melt-cast bioactive glass had a surface area of 5.9 m^2/g and the sol–gel has a surface area of 11.1 m^2/g (95 % reproducibility limit). That is to say, using the sol–gel manufacturing method increased the surface area of the bioactive glass by about a factor of 2. For the purposes of this experiment it was assumed that devitrification of melt-cast bioglass should not significantly change the surface area of the material, relative to the factor of two change in surface area realized for severe morphological differences that exist between the sol–gel and melt-cast derived materials.

3.2 SEM

The morphologies of the bioactive glasses are illustrated in Fig. 1. Gel-derived 45S5 powder appears as agglomerates of fine sub-micron particles and exhibits submicron porosity (Fig. 1a). This leads to a higher surface area for the gel-derived 45S5 compared to the other powders as shown with the surface area results. Melt-cast samples show similar particle morphology in either amorphous or crystalline states (Fig. 1b, c), with crystalline powder having slightly smoother surfaces and edges due to glass softening at relatively high temperatures.

3.3 XRD

X-ray diffraction patterns are shown in Fig. 2. As expected, no sharp peaks were detected on the amorphous

Fig. 1 Secondary electron SEM micrographs of **a** crystalline gel-derived 45S5, **b** amorphous melt-cast 45S5, and **c** crystalline (devitrified) melt-cast 45S5. Notice the agglomerated particles in the gel-derived specimen (**a**) which gives rise to submicron porosity, whereas the melt-cast glasses in (**b**) and (**c**) have much smoother surfaces. Upon heat treatment to change from state (**b**) to (**c**) the glass devitrifies and the sharp angular fractured surfaces smoothen slightly due to glass softening at 720 °C
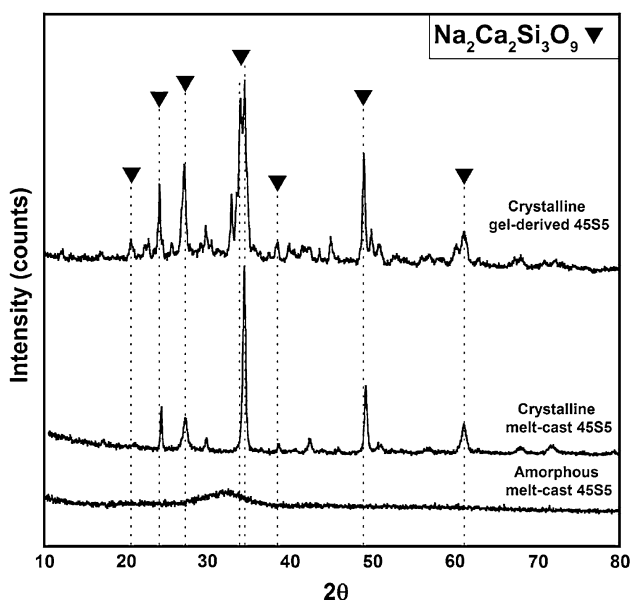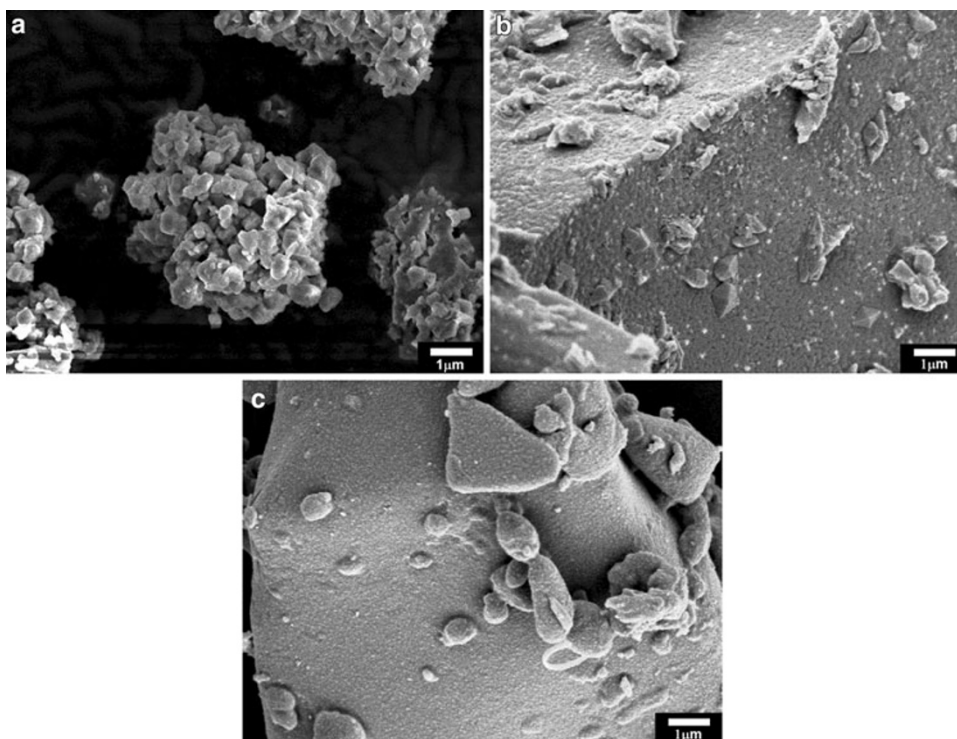
Fig. 2 XRD patterns of melt-cast and gel-derived 45S5 powders. The as cast melt-cast glass is amorphous (showing a broad bump at $\sim 32°$ 2θ and no sharp peaks corresponding to crystallographic planes). When the cast glass is intentionally crystallized the peaks that are observed match those of combeite ($Na_2Ca_2Si_3O_9$), the same phase which is observed after gel-derived 45S5 is thermally stabilized and crystallized

45S5 given its structure; confirmed by the presence of a broad peak at $\sim 32°$ 2θ. The XRD patterns of the crystalline samples matched that of combeite—a crystalline sodium-calcium-silicate phase ($Na_2Ca_2Si_3O_9$, PDF#075-

1687) commonly formed upon devitrification of 45S5 bioactive glass.

3.4 Surface Charge

Zeta potential measurements were conducted on pristine samples to determine the surface charges of the various bioactive glass materials (Table 2). It was observed that all of these materials, regardless of crystallinity or manufacturing conditions, exhibited similar surface charges ranging from -14 to -17 mV. A Student's t test for significance showed that these systems were not statistically different although cast crystalline sample appears to have a difference in surface charge compared to the sol–gel and cast amorphous.

3.5 Surface Properties: X-ray Photoelectron Spectroscopy (XPS) Results

XPS was performed on all systems, both prior to and after incubation in platelet poor human plasma (Table 3).

Table 2 Surface charges of bioactive glass constructs before incubation with human plasma ($n = 3$)

System	Surface charge (mV)
Sol–gel	-14.3 ± 3.5
Cast amorphous	-14.8 ± 2.9
Cast crystalline	-17.1 ± 1.5

Data represent mean ± 1 SD

Table 3 Summary of the atomic percentages of bioactive glass systems before and after incubation with human plasma

System	Na	O	Ca	P	Si	N	C	S
Theoretical (atomic %)	*17.3*	*55.2*	*9.5*	*1.8*	*16.3*			
Before solution incubation								
Sol–gel	9.5	45.7	3.2	0.5	10.7		30.1	
Cast amorphous	8.9	40.9	2.7	1.3	6.1		39.8	
Cast crystalline	7.8	49.1	4.8	0.5	12.3		25.3	
After solution incubation								
Sol–gel	4.5	46.9	7.7	3.6	7.0		29.1	1.1
Cast amorphous	10.7	34.2	2.9	0.8	2.1	1.4	46.6	1.4
Cast crystalline	6.8	53.8	8.9	4.7	8.0		17.3	

Values are accurate to less than ±10 %

Pristine bioactive glass samples showed high levels of carbonaceous contamination, a situation that has previously been reported in the literature for similar systems [35]. The ill-defined layer of contaminating carbon ultimately decreases the atomic percentages of all the other elements, a trend observed for all pristine samples when compared to the theoretical composition. It has been previously shown that carbonaceous contamination may contain oxygen as well, so in order to better understand the bioactive glass surface, the atomic percentages of both carbon and oxygen were removed and the remaining values normalized (Table 4).

High resolution XPS for both Si and P were analyzed. However, the variety of binding energies present for P made it impossible to independently determine its binding environment. A similar issue existed for Si, whereby a plethora of SiOx binding energies have been reported in the literature (ranging from 99.3 to 103.6 eV) [36]. However, the binding energy for SiO was 102.0 eV specifically. Therefore, elucidation of the Si (2p) binding energies was possible; one peak was constrained to represent SiO and a second peak was used to represent the general SiOx binding energies (Table 5). Complimentary to this, a minimum number of peaks were used to fit the high resolution Si data; the reduction of the degrees of freedom in the model, while returning similar fits, being thought to be the most accurate means of modeling this data. Using this strategy for peak fitting of the high resolution Si data, it

was observed that all pristine bioactive glass surfaces had virtually no SiO present. The entire Si (2p) peak could be fit using binding energies relative to SiOx. This might be expected, as it has been discussed in the literature that SiO may be formed only transiently during the early stages of biomineralization [37]. After incubation in plasma both the cast crystalline and sol–gel samples did show some SiO on their surfaces. The presence of SiO on these surfaces but not on the amorphous bioglass suggests that the crystalline samples undergo biomineralization at a slower rate than the amorphous bioactive glass. This increase in reaction time of crystallized bioactive glass is consistent with the literature [10–12].

3.6 Protein Adsorption: Amount Adsorbed

Bioactive glass samples were incubated with platelet-poor human plasma for 2 h at 37 °C and any loosely bound proteins were removed by washing twice with PBS. Rinsed bioactive 45S5 powders were incubated in SDS solutions (final 2 % concentration) and eluents were analyzed for total protein concentration. From the XPS results summarized in Table 3, after incubation in plasma, multiple buffer rinses and the SDS elution step, it was evident that there were only trace amounts of residual N and S on some of the samples.

The total amount of plasma proteins adsorbed to the various bioactive glass systems were determined using two

Table 4 Summary of the atomic percentages of various bioactive glass systems before and after incubation with human plasma after removing C and O values and normalizing

System	Na	Ca	P	Si	N	S
Theoretical (atomic %)	*38.5*	*21.2*	*3.9*	*36.4*		
Before solution incubation						
Sol–gel	39.7	13.5	2.1	44.7		
Cast amorphous	46.8	14.2	6.8	32.2		
Cast crystalline	30.6	18.8	2.0	48.6		
After solution incubation						
Sol–gel	18.8	32.0	15.0	29.1		4.7
Cast amorphous	55.5	15.0	4.1	10.9	7.3	7.2
Cast crystalline	23.5	30.8	16.1	27.8		

Values are accurate to less than ±10 %

Table 5 Summary of high resolution modeling of Si (2p) for bioactive glass samples before and after incubation in plasma

Sample ID	% SiO (102.0 eV)	SiO curve FWHM	% SiO$_x$	SiO$_x$ position (eV)	SiO$_x$ curve FWHM	Possible chemistry	SiO$_x$ references
Before plasma incubation							
Sol–gel	0	0	100	99.8	1.8	Si	[38]
Cast amorphous	0	0	100	99.8	2.0	SiO$_x$/Si	[38]
Cast crystalline	0	0	100	100.9	3.0	SiO$_x$	[39]
After plasma incubation							
Sol–gel	5.5	1.7	94.5	100.2	1.9	SiO$_x$	[39]
Cast amorphous	0	0	100	100.7	2.1	SiO$_x$	[39]
Cast crystalline	25.4	3.1	74.6	100.5	2.0	SiO$_x$	[39]

Values are accurate to less than ± 10 %

Table 6 Protein adsorbed amounts determined using the DC protein assay

System	Concentration of eluted protein (μg/μL)	Eluted protein per Surface area (mg/m^2)
Cast amorphous	0.157 ± 0.004	0.53 ± 0.01
Cast crystalline	0.169 ± 0.01	0.57 ± 0.03
Sol–gel	0.082 ± 0.005	2.46 ± 0.2

Values represent average $\pm$ 1 SD ($n \geq 3$)

Table 7 Protein adsorbed amounts determined using nanogold colourmetric assay

System	Concentration of eluted protein (μg/μL)	Eluted protein per surface area (mg/m^2)
Cast amorphous	0.140 ± 0.007	0.47 ± 0.02
Cast crystalline	0.151 ± 0.007	0.51 ± 0.02
Sol–gel	0.045 ± 0.007	1.35 ± 0.2

Values represent average $\pm$ 1 SD ($n = 3$)

independent methods: the common DC protein assay and an in-house nanogold based assay. DC and nanogold protein assay results are summarized in Table 6 and Table 7, respectively. The nanogold assay was specifically developed to utilize the nanogram sensitivity that Au nanoparticles exhibit for protein, facilitating the quantification of low concentration protein solutions. It is well known that although the DC assay overcomes the issues associated with the presence of SDS in a protein solution, protein concentrations below ~ 0.2 mg/mL (2 % SDS) cannot be accurately detected. Although complicated strategies can be employed for concentrating the protein in solution, a more direct and convenient methodology for directly measuring protein concentration has been employed [23]. Herein, this nanogold assay was shown to be appropriate for quantifying the amount of protein in a concentration range almost five times less that of the minimum detectable concentration of the DC assay, viz., ~ 0.04 mg/mL.

3.7 Protein Adsorption: Adsorbed Proteome

Eluted protein solutions from the various bioactive glass samples were subject to SDS-PAGE and immunoblotting analysis in order to identify the composition of the adsorbed protein layer. In order to facilitate the comparison of band intensities between different systems, a constant quantity of protein (30 μg), as well as constant times for all colour development steps, were used for all systems. This also removes any specific surface area variations when comparing samples. By keeping these conditions constant between samples it is possible to compare the intensities of the immunoblot bands between samples, for the same protein, to determine the relative amount of each protein that was eluted from the bioactive glass surfaces. Table 7 summarizes the band intensity data for all samples. A 13 step grayscale was used to quantify the band intensity. The number 12 indicate a fully black band, or the highest intensity band, and lower numbers mean decreased band intensity. A value of zero indicates no band was present. Moreover, it is not possible to compare between band intensities of different proteins, as each protein may 'label' differently. Thus, only comparisons can be drawn between the intensities of like proteins. It should also be highlighted that although these techniques can detail the composition of the adsorbed protein layer, they do not provide insight into the *conformation* of the adsorbed proteins themselves. Recently, it has been shown that it is not only the adsorbed protein content, but also the conformation of the adsorbed proteins that can facilitate further cellular interactions [40].

The results of the SDS-PAGE of the eluted plasma proteins for each bioactive glass sample seemed quite similar (results not shown). Each of the samples yielded a very intense band at ~ 66 kDa and a moderately intense band at ~ 50 kDa. These bands are thought to be at least partially made up of albumin and alpha$_1$ antitrypsin, respectively. A band at ~ 25 kDa was also visible for each sample, being most intense for the sol–gel system, then the

cast amorphous and least for the cast crystalline systems. Faint banding was also visible at ~35 kDa. In general though, the degree of banding and their intensities in the SDS-PAGE results imply that there were comparable varieties of protein found eluted off of each of the three bioactive glass samples.

4 Discussion

4.1 Surface Area

Surface area measurements indicate twice the surface area per unit mass of powder for sol–gel derived powders compared to melt-cast powders. Based on the manufacturing route, a higher surface area for sol–gels, as their structure is built through condensation of Si–O bonds, leaving behind precursor chemicals which then evaporate leaving pores. The higher specific surface area values for sol–gel powders indicates that the surfaces of such powders should be more tortuous, or more porous than their cast counterparts, which is indeed what was observed in microscopy.

4.2 Sem

SEM confirmed that the powder surface morphology, at least on a micron length scale, was very different between sol–gel and cast powders. The sol–gel powders appear to be agglomerates of submicron particles that have not fully come into contact, thus leaving an internal pore structure on the submicron length scale. The larger melt-cast particles in Fig. 1b and c have smaller powder particles stuck to their surfaces, which also generate regions resembling pores.

With respect to the melt-cast amorphous powder, the weak interaction of smaller powder particles to the surface may or may not be stable in solution, so it is not possible to predict if the specific surface area changes upon immersion. The devitrified melt-cast and stabilized sol–gel powders were exposed to relatively high temperatures (close to the softening temperature/point) so it is reasonable to assume that the powders have fused together with sufficient strength to withstand immersion.

The SEM micrographs also indicate that there is as associated surface roughness on all powder particles. The roughness was not quantified, but judging from the micrographs in Fig. 1 it is possible to see variations in surface roughness of individual particles between the powders; devitrified melt-cast appears smoother than as cast melt-cast powder, and similar to sol–gel powder. Again the thermal treatments likely play a role in the similarity between devitrified melt-cast and sol–gel

powders. Interpretation of fine scale roughness, or smoothness, is not a simple task, and was not undertaken in this work. However, it should be noted that a smoother looking surface could potentially have higher microporosity than a rougher looking surface at low magnifications— the fine scale surface morphology would need to be quantified in order to make any claims about differences between all the powders studied herein in order to shed light on potential implications for porosity on the length scale relevant for proteome adsorption (i.e., nanometer scale). Nonetheless, based on surface area measurements, with gas molecules small enough to penetrate nanometer scale pores, the differences between the powders do not seem great enough to imply large differences in fine scale microporosity on the surfaces of the powders, hence our limited investigation of small scale surface properties.

4.3 XRD

XRD was used to verify the structure of the various powders. The broad peak of the amorphous melt-cast powder indicates that there is no repeating long range order within the glass, and hence there will necessarily be a distribution of bond lengths within the material. For crystalline powders such as devitrified melt-cast powder and sol–gel derived powder the patterns match combeite ($Na_2Ca_2Si_3O_9$), which has a trigonal-trapezohedral class symmetry. A major implication in the formation of combeite crystals in both devitrified powders is that combeite is a calcium sodium silicate and should not contain any phosphorous. If phosphorous was rejected from the combeite crystals as they grew, then a gradient in phosphorous could be generated between the crystals and their grain boundaries, or the phosphorous could volatilize. Previous work has suggested that some phosphorous is still present in a grain boundary phase with different aqueous solubility [17]. XPS analysis suggests that phosphorous content is lower in the crystallized powders (Table 4), which could imply that some of the phosphorous has volatilized, and that some remains in the grain boundary phase. Regardless, the phosphorous effect is likely not significant; similar XRD patterns and surface chemistry (XPS) between crystalline powders does not result in similar protein adsorption profiles, thus the surface morphology, or more subtle variations in surface chemistry may play a more dominant role.

4.4 Surface Charge: Zeta Potential

The zeta potential results differ from those reported by El-Ghannam et al. [41] where they show that for cast amorphous 45S5 bioactive glass as little as 5 % crystallization of cast amorphous bioactive glass leads to a statistically significant change in zeta potential. It should be

noted that in the study performed by El-Ghannam et al. the bioactive glass particulates were suspended in simulated body fluid, which may alter the surface properties.

4.5 Surface Properties: XPS

It is apparent that substantial differences existed between the fractional amount of various elements predicted by the overall atomic composition of the bioactive glass samples and the atomic compositions determined at the surface region using XPS techniques. Theoretically, all bioactive glass samples should have similar surface compositions; however, it was observed that the surface regions had somewhat unique atomic profiles. In general, the pristine sol–gel surface was enriched by ~ 23 % in Si, compared to the theoretical content, while being depleted by ~ 36 and 46 % in Ca and P, respectively (Table 4). These are obviously substantial differences in the surface content of the sol–gel materials. The surface of the pristine cast amorphous sample showed an enrichment of ~ 22 and 74 % in Na and P specifically, while exhibiting a reduction of ~ 33 % in Ca. Upon crystallization, however, cast crystalline samples were observed to be enriched by ~ 34 % in Si and reduced by ~ 20 and 49 % in Na, and P, respectively.

The crystallization of 45S5 bioactive glass seemed to have dramatic effects upon the atomic composition of the surfaces. For example, when comparing the cast amorphous to cast crystalline it is apparent that the levels of Na and Si are almost exactly reversed. The cast crystalline having ~ 49 % of the surface composed of Si, while the amorphous material exhibiting ~ 47 % of the surface being Na. Also of interest is the apparent difference in P, where the amorphous layers had more than three times the P than either crystalline material. Moreover, it seems that the surface compositions of the cast crystalline and crystalline sol–gel were somewhat similar: both showed enriched amounts of Si, and similar amounts of P. The only substantial differences being that the sol–gel surfaces retained more Na and less Ca than the cast crystalline samples. Currently there are very few XPS measurements for the sol–gel derived bioactive glass, making it difficult to compare these results to the literature.

The pristine bioactive glass elemental composition data only somewhat resembles the XPS data for the cast amorphous 45S5 bioactive glass found in the literature [35, 42] most likely due to the differences in the amounts and thicknesses of C and O contamination and their effects on the atomic concentration calculations and the penetrating power of the XPS itself. Chen et al. had C and O levels of 49.6 % and 24.8 % respectively and Mladenovic et al. found C levels of 12.3 % and O levels of 66.05 % on their respective cast amorphous 45S5 bioactive glass. Not only

are these values different from those shown in Table 3 and from one another, the levels of Na, Ca, P and Si reported in [35, 42] also vary a considerable degree. Chen et al. report atomic concentrations of 0.88, 4.63 and 4.03 % for Na, Ca and P respectively while Mladenovic et al. found their surfaces composed of 16.27, 2.91 and 0.25 % Na, Ca and P.

It is well known that the incubation of bioactive glass samples (amorphous) in various 'physiologically relevant' solutions (i.e., simulated body fluid) leads to the first steps of biomineralization, as aptly reviewed elsewhere [9]. From this work, it is also apparent that incubation in platelet-poor human plasma affected the surface composition of each of the bioactive glass samples. Upon comparing the pristine sol–gel with the same samples after incubation in plasma it is apparent that drastic differences in all atomic concentrations occurred. After incubation the sol–gel surface layers experienced respective reductions of ~ 52 and 35 % in Na and Si content. Conversely, the sol–gel surfaces experienced drastic increases of ~ 2 and 7 times for Ca and P content. These changes in surface chemistry correlate with the sequence of events which occur on bioactive glass surfaces during bone bonding [9]. The apparent reduction in Na^+ is more accurately described as an exchange of cations with H^+ or H_3O^+ from solution. The decrease in Si is consistent with the loss of soluble SiO_2 species and the large increases in surface Ca and P match the composition of naturally grown apatites and indicate the first step of hydroxyapatite formation [9]. Lastly, the presence of S atoms was most likely due to remaining sodium dodecyl sulfate (SDS), which was used as a detergent to strip proteins off of these surfaces. Cast amorphous surfaces, however, did not exhibit a drastic alteration in atomic concentrations. Only moderate changes in Na and decrease in P were observed, most likely within the error of the characterization technique. However, a Si decrease of ~ 60 % occurred. Again this is consistent with the dissolution of SiO_2 seen in the sol–gel sample but could also indicate that the XPS is not penetrating far enough into the material to reach the Si rich layer as shown in [9]. This could be explained by the presence of an N and S signal for these samples, suggesting the presence of protein and the potential presence of SDS. This adsorbed layer of biomolecules could inhibit the signal intensity of the bioactive glass surface atoms. Cast crystalline surface alterations were very similar to those observed for the sol–gel surface, showing drastic increases of ~ 2 and 7 times the amount of Ca and P, respectively, and a decrease of ~ 43 % in Si as well. As with the sol–gel bioactive glass, the decrease in Si may be indicative of the loss of soluble SiO_2 species and the large increases in Ca and P suggest the accumulation of the chemical moieties necessary for hydroxyapatite formation [9]. Although not guaranteed, in this case it would

seem a complete removal of SDS and protein occurred, as evidenced by the lack of N and S signal. Moreover, it was apparent that the two crystalline materials underwent very similar changes in their surface chemistry and those changes were not consistent with those seen for the cast amorphous bioactive glass.

In order to further understand the state of the surface, it is important to consider the steps of interfacial reactions that are thought to occur in solution after 3 h incubation in platelet poor human plasma. Previous work has detailed the sequence of reactions at the bioactive glass surface [9]. Briefly, bioactive glasses first experience dissolution of Na^+ and/or K^+ with H^+ or H_3O^+ in solution. Silanol (SiH_3OH) formation is thought to occur next, in conjunction with the release of soluble SiO_2. These silanol groups undergo further polycondensation, and the material begins to adsorb amorphous phosphates, calcium and carbonate groups from solution. These groups then undergo crystallization to form hydroxyl carbonate apatite. These first steps taking place within the first 2 h of solution incubation for amorphous 45S5 bioactive glass [9]. The next step is adsorption of biological moieties to the newly formed hydroxyl carbonate apatite layer. This step is thought to occur as early as the polycondensation of silanol groups and continues throughout crystallization until the action of macrophages is observed after ~ 15 h solution incubation.

Upon comparison of the changes in surface composition data of the cast crystalline and sol–gel samples as well as the results of the Si modeling to the same timeline of surface reaction it can be said that the increases in surface Ca and P suggest that the first steps of biomineralization have been completed and the materials were most likely adsorbing amorphous Ca, PO_4 and CO_3 [9]. Furthermore, the SiO found on the same surfaces means that both the sol–gel and cast crystalline samples are still undergoing polycondensation of SiOH and adsorption of Ca and P as discussed above. Determining the position of the cast amorphous bioactive glass on the timeline was more difficult in that the XPS data only showed a decrease in Si and increases in S and N after incubation in plasma. The lack of detectable SiO on the surface of the cast amorphous sample could mean that the sample has not undergone any surface biomineralization reactions or that is has moved beyond the polycondensation step. As discussed above, the decrease in Si could be attributed to SiO_2 dissolution or may be a result of changes in the surface profile of the sample as adsorption of hydroxyl carbonyl apatite components occurred. At hour 3 of the interfacial reaction timeline the adsorption of the components of hydroxyl carbonyl apatite has ceased and the crystallization of these components is complete. The primary active process is the adsorption of various biological entities, such as proteins, to the newly formed hydroxyl carbonyl apatite layer. This may be reflected in

the results by the presence of N and S, elements indicative of proteins. Furthermore, the similarity of the Si signals for cast amorphous bioactive glass before and after incubation is consistent with what has been observed the literature [43].

When the positions of the three bioactive glass samples on the interfacial reaction timeline are compared to each other it is clear that this series of experiments demonstrates that all bioactive glass samples have begun biomineralization with the cast amorphous sample progressing at the rate predicted in the timeline for a 3 h incubation and the cast crystalline and sol–gel samples lagging behind. This is consistent with the findings of Filho et al., which state that crystallization of 45S5 bioactive glass slows the rate of surface reactions but does not completely halt them [44].

4.6 Protein Adsorption: Amount Adsorbed

When considering the adsorbed amounts calculated, it is imperative that the surfaces areas were determined using B.E.T. gas (N_2) adsorption. Given the probability that surfaces accessible to this gas may not be accessible to proteins, makes it very difficult to accurately determine the amount adsorbed per unity surface area. Nevertheless, this strategy was adopted due to the fact that it is unknown how much of this surface area is accessible to the solvent and available for protein interactions. In general, when near the lower concentration limit of the DC assay (~ 0.2 mg/mL), both the DC and colloidal gold assays yielded similar concentrations. However, a large difference occurred when attempting to quantify protein concentrations lower than the suggested minimum for the DC assay. The DC assay showed, for the sol–gel prepared surfaces, a total protein concentration almost twice as large as the nanogold assay technique. It is thought that this difference was largely due to the inaccuracy of the DC assay at this concentration. Nevertheless, it is apparent that the cast amorphous and cast crystalline samples had similar amounts of protein removed from their surfaces and that these values were at least double that of the amount adsorbed to the sol–gel sample before considering the specific surface area of the samples. When the amount of surface area of each sample is taken into account, the relationship is then inverted and the sol–gel bioactive glass eluted more protein per unit mass than the cast samples. These results show that the devitrification of melt-cast 45S5 does not play a significant role in the adsorption of plasma proteins as both the cast amorphous and cast crystalline samples eluted similar quantities of protein. Data in Table 3 suggests the elution procedure may not have been 100 % complete as based on the atomic percentages of nitrogen and sulphur. Despite these values being only approximately 1 %, it is probable that they represent both retained protein (N and S) and/or

SDS (S) on the material surface. However, due to their low levels and the lack of consistent trend in the C or O amounts, the amount of trace protein left at the powder surface was thought to be minimal.

4.7 Protein Adsorption: Adsorbed Proteome

Elucidating the underlying reasons for the presence of different proteins screened for using immunoblot techniques is not a trivial task. The complexity of the surface, relative to the diversity of the proteins in solution makes it almost impossible to attribute a proteins presence at the interface due to charge differences between the protein and surface only. In reality, proteins adsorbed to the interface may facilitate further protein adsorption. This is compounded further due to the fact that bioactive glass, upon immersion into plasma, has been shown to have a transient interfacial composition. Thus, the best that can be done is to understand the types of proteins present, their relative amounts, and potential influence for the various bioactive glass preparations.

The data in Table 8 shows a clear difference in the identities of the proteins adsorbed to either crystalline 45S5 samples. This change in protein profile cannot be attributed to the difference in specific surface area as identical amounts of eluted protein were used in the Western analysis. Furthermore, given the very high sensitivity of the Western blotting technique it is unlikely that any plasma proteins present would not be detected. Thus the only reason for such a large variation in plasma protein adsorption between crystalline 45S5 samples would be their surface compositions, or surface morphology, both of which could affect protein conformation.

After albumin has been denatured and reduced during sample preparation for SDS-PAGE the protein runs as a single band with a molecular weight of 66 kDa. Albumin was found to be in the eluted protein solutions for all samples. Moreover, the band intensities indicated that albumin was present at a similar amount for all samples studied; with the cast amorphous sample potentially adsorbing less than both cast crystalline and sol–gel samples. From this data, it is also apparent that even though there was more protein adsorbed in total to the cast samples, the protein layer present for these systems was largely composed of albumin. In the case of cast crystalline this was the only protein that was observed to be present, and cast amorphous this was one of only two proteins observed: out of the 23 proteins screened. The presence of albumin is somewhat expected due to its high plasma concentration, but it is of particular interest due to the fact that it has been reported that denatured albumin can lead to platelet adsorption and activation [40]. This is particularly important, as activated platelets are commonly used for bone formation strategies [45].

Complement refers to a portion of innate immunity that when activated can cause opsonization, an increased antibody response and lysis of cells [46]. As it is a response to foreign bodies and materials, complement activation can have serious consequences for biomaterial effectiveness and overall host health [47]. Central to each of the three complement activation pathways is complement Factor 3 (C3) [46]. It is composed of α (115 kDa) and β (72 kDa) peptide chains, respectively. If complement is activated and C3 cleaved, a band at 42 kDa becomes apparent [46]. Given this, it was apparent that the different surfaces adsorbed varying amounts of C3 and showed differences in activation of the complement pathway. The sol–gel sample showed high levels of all of the C3 fragments, indicating that this surface strongly adsorbed and activated C3; possibly indicating this surface may illicit a strong immune response. The cast amorphous system showed less amounts

Table 8 Relative intensities for immunoblots of plasma proteins eluted from all of the bioactive glass systems investigated

0 indicates zero band intensity. The number 12 indicates the highest intensity band, with lower numbers indicating lower intensity

Plasma protein	Fragment size (kDa)	Fragment name	System		
			Cast amorphous	Cast crystalline	Sol–gel
Albumin	66		9	12	12
C3	42	Activation	4	0	9
	70	β	8	1	12
	115	α	3	0	12
IgG	27	Light	0	0	4
	55	Heavy	0	0	1
Alpha$_1$ antitrypsin	47		6	1	11
Fibrinogen	48	γ	0	0	0
	56	β	0	0	9
	68	α	0	0	9
	<48	Cleavage	0	0	0
Transferrin	77		0	0	11
Antithrombin	53		0	0	9

of adsorbed and activated C3, but more than cast crystalline samples. The cast crystalline sample was found to have almost no detectable C3 on its surface. Only a small amount of the β chain was found. This information may imply that the cast crystalline samples will not strongly activate complement in vivo, while the other two samples may.

Immunoglobulin G (IgG) is an antibody involved in host immune response that, upon binding to an antigen, can cause opsonization and phagocytosis and complement activation via the classical pathway [46]. IgG normally runs as two bands: the heavy chain at 55 kDa and the light chain at 27 kDa. Neither the cast amorphous nor cast crystalline samples appeared to have any IgG on their surfaces. However, this protein was found eluted off of the surface of the sol–gel system. Although IgG was detected, other critical molecular markers for indicating a potential immune response were not observed to be present. For example, the lack of Factor I may indicate that although IgG was present, the classical activation pathway may not be initiated (Table 7). Of course, this does not rule out the possibility of IgG opsonization, and potential phagocytosis or fibrous capsule formation occurring due to the presence of IgG; as previously observed for cast 45S5 bioactive glass systems implanted into the thigh muscles of Sprague–Dawley rats [48].

Alpha$_1$-antitrypsin is considered to be one of the most important serine proteases in the body [49] and is responsible for maintaining anti-inflammatory response (especially in protecting connective tissues). Normally, alpha$_1$-antitrypsin appears as a single band at ~ 52 kDa. In general, this plasma protein was found to elute off of all of the tested samples. The cast crystalline sample showed the least amount of the protein, followed by the cast amorphous. The sol–gel sample had the highest amount of alpha$_1$-antitrypsin found in the adsorbed protein layer. Given that alpha$_1$-antitrypsin has a charge of -12 at a pH of 7.0, it might not be expected that its adsorption to negatively charged bioactive glass should be observed. However, two possible mechanisms may allow for this to occur. Firstly, this protein is a part of the adsorbed protein layer, and may interact with already adsorbed protein as opposed to directly interacting with the surface. Secondly, the composition of the surface of the bioactive glass is transient as it incubates within the plasma solution.

Fibrinogen's α, β and γ chains appear as three bands with molecular weights of 68, 56 and 48 kDa, respectively. Bands at lower molecular weights can appear when fibrinogen is cleaved. The sol–gel bioactive glass is the only sample from which any fibrinogen was eluted. While the lack of fibrinogen degradation products may seem to be a positive sign in that the surface does not appear to stimulate fibrin formation, adsorbed fibrinogen has been shown to denature to the point where it resembles fibrin or fibrinogen degradation products [50]. Additionally adsorbed fibrinogen can activate platelets [51] and has been shown to cause the accumulation of phagocytes [52], which fight infection.

Transferrin is primarily responsible for the transport of iron [53], and when run on a reduced SDS-PAGE gel it forms a single band with an approximate molecular weight of 75 kDa [53]. Transferrin was found exclusively on the surface of the sol–gel sample. Based on its relative band intensity, a large amount of transferrin was removed from the bioactive glass surface. Given that the protein does not contain a large number of charged residues it can be presumed that the transferrin was not adsorbed due to charge–charge interactions.

Antithrombin is a serine protease inhibitor and while not limited to acting on thrombin it is one of the most important proteins responsible for limiting irregular clotting [54].

This protein appears as a single band at approximately 53 kDa when run on an SDS-PAGE gel. It was found on the sol–gel bioactive glass in fairly high amounts as determined by the relative band intensity. As was the case with transferrin this protein is not charged and was only found on the sol–gel bioactive glass. Given that both the sol–gel and cast crystalline bioactive glass samples are crystalline and have similar surface compositions (Table 3) some characteristic imposed upon the sol–gel sample during its manufacturing appears to be the cause of anti-thrombin adsorption. When comparing to the XPS data, it seems that antithrombin's adsorption differences between these samples cannot be due to the biomineralization process, for if it were it should be found on both the cast crystalline and sol–gel samples as they are at roughly the same place in their maturation.

The absence of proteins from the bioactive glass surfaces can provide just as much information as the proteins found on the surface. When comparing the list of proteins found on the various bioactive glass surfaces (Table 7) to the table listing all of the proteins which were scanned for (Table 1) there are a large number of important plasma proteins which were not found on any of the surfaces. Of significance is the lack of any common cell adhesive proteins (i.e., fibronectin and vitronectin) being present on the surfaces. The presence of fibronectin has never been found on the surfaces of pristine bioactive glasses [55]. As for clot formation, Factor XI, Factor XII, prekallikrein and high molecular weight kininogen are all absent. These contact phase coagulation proteins are involved in the initiation of the extrinsic coagulation cascade. Their lack of detection may indicate that none of the samples may activate coagulation through the contact phase. Neither prothrombin nor thrombin was found on the surfaces of any of the bioactive glass samples. This is another strong

indication that these surfaces do not stimulate coagulation given thrombin's central role in this process [54]. Furthermore, the lack of these proteins in conjunction with protein C and protein S indicates there is no strong anticoagulant activity caused by the bioactive glass samples. Also, the absence of α_2-macroglobulin, a potent inhibitor for both clotting and fibrinolysis, further strengthens the hypothesis that the bioactive glass surfaces do not stimulate either clot formation or breakdown. These are generally considered a positive attribute for implanted biomaterials to have, as the lack of these molecular level markers for the activation of the coagulation cascade may indicate a lack of clot formation.

While the consequences of the adsorption of specific plasma proteins on cellular responses such as osteoblast differentiation, viability and proliferation are beyond the scope of this study, it has been demonstrated that a multitude of factors influence plasma protein adsorption and, by extension, host response. This has been unwittingly demonstrated in the literature by the varied responses of osteoblasts to Class A bioactive materials. The effects of these materials have ranged from very positive to inhibitory [23–27]. Given that these studies did not use identical circumstances or times, they also would not have elicited identical responses from the plasma proteins directing host responses.

5 Conclusions

In this study bioactive glass 45S5 was produced in various forms using differing methods and evaluated for their physical characteristics and interactions with platelet poor human plasma. Commercially and medically employed melt-cast 45S5 was compared with devitrifed crystalline melt-cast 45S5 as well as sol–gel produced crystalline 45S5. These modifications in bioactive glass synthesis were imparted to produce glasses with better physical properties. Devitrification of melt-cast 45S5 leads to improved mechanical properties while enabling powder sintering and using the sol–gel method produces a porous crystalline glass with a higher specific surface area to encourage interactions with the surrounding environment.

It was found that sol–gel derived 45S5 showed higher surface area and submicron porosity in the structure compared to either of the melt-derived glasses. This in turn led to increased plasma protein adsorption both in terms of quantity and in variety of the adsorbed proteome. The presence of IgG and fibrinogen on the sol-gel glass suggest that this manufacturing method may lead to negative host responses, namely immune and clotting responses. The devitrification of melt-cast 45S5 changed the surface composition as shown by XPS analysis but did not change

the amount of plasma protein adsorption; devitrification did, however decrease the presence of C3 and alpha$_1$ antitrypsin on the surface which may decrease any tendency toward deleterious host responses. These differences in surface structure obviously affect the adsorbed proteome and may influence bone integration via mediating cell attachment.

References

1. Hench L, Splinter R, Allen W, Greenlee T (1971) J Biomed Mater Res 5:117–141
2. Hench LL, Paschall HA (1973) J Biomed Mater Res 7:25–42
3. Ogino M, Hench LL (1980) J Non-Cryst Solids. 38–39 Part 2:673–678
4. Hench LL (1996) Ceram Int 8842(95):493–507
5. Xynos ID, Hukkanen MVJ, Batten JJ, Buttery LD, Hench LL, Polak JM. Bioglass 45S5 (2000) Stimulates osteoblast turnover and enhances bone formation in vitro: implications and applications for bone tissue engineering. New York, pp 321–329
6. Gough JE, Notingher I, Hench LL (2004) J Biomed Mater Res Part A 68:640–650
7. Christodoulou I, Buttery LDK, Saravanapavan P, Tai G, Hench LL, Polak JM (2005) J Biomed Mater Res B Appl Biomater 74:529–537
8. Christodoulou I, Buttery LDK, Tai G, Hench LL, Polak JM (2006) J Biomed Mater Res B Appl Biomater 77:431–446
9. Hench LL (1998) J Am Ceram Soc 81:1705–1728
10. Greenlee TK Jr, Beckham CA, Crebo AR, Malmorg JC (1972) J Biomed Mater Res 6(3):235–244
11. Peitl O, La Torre GP, Hench LL (1996) J Biomed Mater Res 30(4):509–514
12. Peitl O, Zanotto ED, Hench LL (2001) J Non-Cryst Solids 292(1–3):115–126
13. Kokubo T, Takadama H (2006) Biomaterials 27(15):2907–2915
14. Hench LL, Jones JR (2002) Bioactive Materials for Tissue Engineering Scaffolds. In: Pollak JM, Hench LL, Kemp P (eds) Tissue Engineering: World Scientific Pub. Co Inc., pp 3–24
15. Lefebvre L, Gremillard L, Chevalier J, Bernache-Assolant D (2008) Sintering behavior of 45S5 Bioglass (R). Bioceramics, Vol 20. Pts 1 and 2, pp 265–268
16. Lefebvre L, Chevalier J, Gremillard L, Zenati R, Thollet G, Bernache-Assolant D, Govin A (2007) Acta Mater. 55:3305–3313
17. Nychka JA, Mazur S, Kashyap S, Li D, Yang FQ (2009) JOM-US. 61:45–51
18. Chen QZ, Thompson ID, Boccaccini AR (2006) Biomaterials. 27:2414–2425
19. Li R, Clark A, Hench LL (1991) J Appl Biomater. 2:231–239
20. Jones JR, Sepulveda P, Hench LL (2001) J Biomed Mater Res 58(6):720–726
21. Pirayesh H (2010) Effects of manufacturing method on surface mineralization of bioactive glasses. Edmonton: University of Alberta, Department of Chemical and Materials Engineering

22. Kokubo T, Kushitani H, Sakka S, Kitsugi T, Yamamuro T (1990) J Biomed Mater Res 24:721–734
23. El-Ghannam A, Ducheyne P, Shapiro IM (1997) Biomaterials 18(4):295–303
24. Wilson J, Pigott GH, Schoen FJ, Hench LL (1981) J Biomed Mater Res 15:805–817
25. Vrouwenvelder WCA, Groot CC, de Groot K (1992) Biomaterials. 13(6):382–392
26. Matsuda T, Yamauchi K, Ito G (1987) J Biomed Mater Res 21:499–507
27. Vrouwenvelder W, Groot C (1993) J biomed. 27:465–475
28. Brash JL (2000) J Biomater Sci Polym Ed 11:1135–1146
29. Kaufmann EA, Ducheyne P, Radin S, Bonnell DA, Composto R (2000) J Biomed Mater Res 52:825–830
30. Buchanan LA, El-Ghannam A (2010) J Biomed Mater Res Part A. 93(2):537–546
31. Singh HD, Wang G, Uludağ H, Unsworth LD (2010) Acta biomaterialia 6:4277–4284
32. Taylor JA, Lancaster GM, Ignatiev A, Rabalais JW (1978) J Chem Phys 68:1776
33. Kim HR, Andrieux K, Gil S, Taverna M, Chacun H, Desmaële D et al (2007) Biomacromolecules 8:793–799
34. Unsworth LD, Sheardown H, Brash JL (2005) Biomaterials 26:5927–5933
35. Chen QZ, Rezwan K, Armitage D, Nazhat SN, Boccaccini AR (2006) J Mater Sci Mater Med 17:979–987
36. NIST (2003) X-ray Photoelectron spectroscopy database (database on the Internet) (cited November 2010). Available from: http://srdata.nist.gov/xps/
37. Hench LL (1998) Feature 1705. Stress: Int J Biol Stress: 28
38. Cros A, Saoudi R, Hollinger G, Hewett Ca, Lau SS (1990) J Appl Phys: 1826
39. Aoyama T, Sugii T, Ito T (1989) Appl Surf Sci 41:584–586
40. Sivaraman B, Latour RA (2010) Biomaterials 31:1036–1044
41. El-Ghannam A, Hamazawy E, Yehia A (2001) J Biomed Mater Res 55(3):387–395
42. Mladenovic Z, Sahlin-Platt A, Bengtsson A, Ransjö M, Shchukarev A (2010) Surf Interface Anal 42(6–7):452–456
43. Cerruti M, Bianchi CL, Bonino F, Damin A, Perardi A, Morterra C (2005) J Phys Chem B 109:14496–14505
44. Peitl Filho O, LaTorre GP, Hench LL (1996) J Biomed Mater Res 30:509–14
45. Anitua E, Andia I, Ardanza B, Nurden P, Nurden AT (2003) Thromb Haemostasis: 4–15
46. Molina H (2004) Rheum Dis Clin N. Am 30:1–18
47. Tang L, Liu L, Elwing HB (1998) J Biomed Mater Res 41:333–340
48. Clark AE, Hench LL, Paschall HA (1976) J Biomed Mater Res 10(2):161–174
49. Gettins PGW (2002) Chem Rev 102:4751–4804
50. Mosesson MW (2005) J Thromb Haemostasis (JTH) 3(8):1894–1904
51. Massa TM, Yang ML, Ho JYC, Brash JL, Santerre JP (2005) Biomaterials 26:7367–7376
52. Tang L, Eaton JW (1999) Mol Med 5:351
53. Moos T, Morgan EH (2000) Cell Mol Neurobiol 20:77–95
54. Davie EW, Kulman JD (2006) Sem Thromb Hemostasis 32:3–15
55. El-Ghannam A, Ducheyne P, Shapiro IM (1999) J Orthop Res 17:340–345